β-sheet-like formation during the mechanical unfolding of prion protein

Weiwei Tao, Gwonchan Yoon, Penghui Cao, Kilho Eom, and Harold S. Park

---

Articles you may be interested in

Exploring the role of hydration and confinement in the aggregation of amyloidogenic peptides Aβ16−22 and Sup357−13 in AOT reverse micelles
J. Chem. Phys. **141**, 22D530 (2014); 10.1063/1.4902550

Relationship between disease-specific structures of amyloid fibrils and their mechanical properties
Appl. Phys. Lett. **102**, 011914 (2013); 10.1063/1.4774296

Protein mechanical unfolding: Importance of non-native interactions
J. Chem. Phys. **131**, 215103 (2009); 10.1063/1.3272275

Mechanical unfolding of proteins L and G with constant force: Similarities and differences
J. Chem. Phys. **131**, 045102 (2009); 10.1063/1.3183974

Mechanical unfolding of ubiquitin molecules
J. Chem. Phys. **123**, 194903 (2005); 10.1063/1.2046609

β-sheet-like formation during the mechanical unfolding of prion protein

Weiwei Tao,[1] Gwonchan Yoon,[1,2] Penghui Cao,[1] Kilho Eom,[3] and Harold S. Park[1,a)]

[1]*Department of Mechanical Engineering, Boston University, Boston, Massachusetts 02215, USA*
[2]*Department of Mechanical Engineering, Korea University, Seoul 136-701, South Korea*
[3]*Biomechanics Laboratory, College of Sport Science, Sungkyunkwan University,*
Suwon 16419, South Korea

Single molecule experiments and simulations have been widely used to characterize the unfolding and folding pathways of different proteins. However, with few exceptions, these tools have not been applied to study prion protein, PrP^C, whose misfolded form PrP^{Sc} can induce a group of fatal neurodegenerative diseases. Here, we apply novel atomistic modeling based on potential energy surface exploration to study the constant force unfolding of human PrP at time scales inaccessible with standard molecular dynamics. We demonstrate for forces around 100 pN, prion forms a stable, three-stranded β-sheet-like intermediate configuration containing residues 155-214 with a lifetime exceeding hundreds of nanoseconds. A mutant without the disulfide bridge shows lower stability during the unfolding process but still forms the three-stranded structure. The simulations thus not only show the atomistic details of the mechanically induced structural conversion from the native α-helical structure to the β-rich-like form but also lend support to the structural theory that there is a core of the recombinant PrP amyloid, a misfolded form reported to induce transmissible disease, mapping to C-terminal residues ≈160-220. © 2015 AIP Publishing LLC. [http://dx.doi.org/10.1063/1.4931819]

I. INTRODUCTION

Prion diseases or transmissible spongiform encephalopathies (TSEs), including bovine spongiform encephalopathy (BSE) in cattle, scrapie in sheep, chronic wasting disease (CWD) in cervids, and Creutzfeldt-Jakob's disease (CJD) and Kuru in humans are fatal neurodegenerative diseases.[1,2] These diseases are associated with the conversion of innocuous cellular prion protein (PrP^C) to an infectious scrapie form (PrP^{Sc}) which can aggregate into a variety of forms of amyloid plaques in the brain. The mature human PrP (huPrP, 23-230) has an unstructured N-terminus domain (23-124) and a globular domain (125-228) containing three α-helices (HA, 144-156, HB, 174-194, HC, 200-228) and a short β-sheet (S1, 129-132, S2, 160-163) with a disulfide bond between C179 and C214 linking HB and HC.[3,4] The conversion of PrP^C to PrP^{Sc} is believed to involve a decrease of α-helix content and a subsequent increase of β-structure.[5–7] Although various models of PrP^{Sc} have been proposed, the structure of PrP^{Sc} remains unsettled and controversial due to issues with experimentally resolving its three-dimensional structure.[8–10] In particular, it has not been determined how the native, helical PrP^C structure transforms into the β-sheet-rich PrP^{Sc} form.

Most studies of PrP have focused on chemical means to induce folding, unfolding, and misfolding, which include low pH, high temperature, or chemical denaturant.[11–15] However, the usage of mechanical force to study PrP has only recently been done,[16–19] though single molecule force spectroscopy has been used to study protein unfolding over the past

20 years.[20,21] Mechanical denaturation of protein has certain advantages over chemical denaturation, namely, that solution conditions such as pH and temperature can be kept constant while the protein dynamics occur such that the key factors controlling misfolding can be studied in isolation. Moreover, mechanical denaturation allows for finding the intermediate conformations that are sometimes inaccessible with chemical denaturation.[22] Also, PrP can be unfolded by mechanical force *in vivo* when being translocated or retranslocated across the endoplasmic reticulum.[23] Ganchev *et al.* performed a single-molecule pulling experiment of amyloid fibrils formed by human PrP 90-231 (huPrP 90-231) using an atomic force microscope (AFM). Interestingly, they were able to identify a stable β-sheet core starting at residues ≈164-169.[19] More recently, single molecule force spectroscopy was used by Yu *et al.* to study the mechanical misfolding of PrP.[16–18] They reported the observation of three misfolding pathways that originated from the unfolded configuration.[17]

However, due to experimental uncertainties with regard to the unfolding and folding pathways as well as the structure of the intermediate configurations,[18] computational atomistic modeling can play a needed role in elucidating potential routes to formation of the scrapie form.[24] Various atomistic simulation techniques including classical molecular dynamics (MD), normal mode analysis, replica exchange molecular dynamics as well as other enhanced molecular dynamics techniques have been used to study the PrP^C to PrP^{Sc} transition.[12,25,26] However, none of these studies have involved unfolding under the influence of mechanical forces. Furthermore, while many interesting and potentially important insights into prion behavior have been obtained from the MD simulations, we note the known limitation of MD simulations in that the time scales they

---

a)Author to whom correspondence should be addressed. Electronic mail: parkhs@bu.edu

can access, i.e., hundreds of nanoseconds, is typically much shorter than the time needed to unfold and refold a protein,[27] though recent MD simulations using GPU computing have been able to reach time scales on the order of a few microseconds.[28] Therefore, important issues such as the structure and configuration of intermediate states for prion, as well as the mechanisms by which the transition from the α-rich form to β-rich form occurs, remain unresolved.

In this work, we employ the recently developed self-learning metabasin escape (SLME) method,[29–31] which couples potential energy surface exploration with constant applied forces, to study the mechanical unfolding of huPrP 125-228[29,30,32] with experimentally relevant forces (around 100 pN) and time scales (microseconds) at neutral pH. Our key finding is that in this force range, PrP forms a three-stranded β-sheet-like intermediate state in the C-terminal starting from residue 155 and extending to the disulfide bond C214. We also considered the mechanical unfolding of mutated human PrP, C179A/C214A, as it has been reported that removal of the disulfide bond can cause conformational changes leading to misfolding similar to that seen in low pH. Our simulations show that while mutated PrP becomes less mechanically stable, the observation of the same three-stranded intermediate state suggests that it is possible for the mutant to convert into the β-rich form and thus that residues 155-214 may play an essential role in the conversion of PrP^C to PrP^{Sc}. Therefore, our simulations not only show the atomistic details of the mechanically induced structural conversion from the native α-helical structure to the β-like-rich form but also lends support to the structural theory that there is a core of the recombinant PrP amyloid mapping to C-terminal residues $\approx$160-220 as reported by Cobb *et al.*[10,33]

II. RESULT

A. Wild-type PrP

All results were obtained using the SLME method,[29,30] which was recently utilized to develop new insights into the mechanical unfolding mechanisms of ubiquitin.[31] The details of the method are given in the Appendix, while the validation of unfolding pathways against steered molecular dynamics (SMD) simulations is given in the supplementary material.[49]

Specifically, we have verified that the SLME method gives the same unfolding pathways as SMD at high (i.e., $\geq$200 pN for wild-type PrP) clamping forces. As shown in Fig. S4(a),[49] the unfolding times obtained using the SLME method are also comparable to the SMD obtained values in the high force regime. The unfolding time is force-dependent and increases as the force decreases, with the unfolding time at 100 pN being on the order of microseconds for wild-type PrP (WT PrP).

Having established the ability of the SLME method to match the MD observed unfolding times in the high force regime as can be seen in Fig. S2,[49] we focus our discussion on unfolding at 100 pN, as experimental studies have been performed in this force range.[19] To get a statistical representation of the unfolding pathways, 30 independent unfolding simulations with a clamping force of 100 pN were performed for WT PrP. We observe that nearly all of the 30 simulations with 100 pN clamping forces pass through intermediate configurations.

We now proceed to characterize the intermediate states that we observed using the SLME method, which can be seen in Fig. 1. Specifically, two intermediate states were observed for the 100 pN clamping force, with end-to-end extensions around 3 nm and 13.5 nm. Fig. 2(a) shows the contact map of hydrogen bonds for WT PrP at 100 pN clamping force as well as the corresponding atomic structures of the native state, the intermediate state emerging during the breakage of the initial β sheet at about 3 nm extension, and the intermediate configuration at 13.5 nm extension as shown in Fig. 1. Fig. 2(c) shows the dynamic behavior of secondary structure transitions such as the $\alpha-\beta$ transition for WT PrP under 100 pN clamping force.

The unfolding pathway at 100 pN shown in Fig. 1 starts from the unfolding of HC and the breakage of the native β-sheet, which happens around 6 μs (t_0) as shown in Figs. 2(aII) and 2(c). However, the native β-sheet does not unravel directly. Instead, newly formed main chain hydrogen bonds S132-V161, M134-N159, and S135-N159 extend the native β-sheet whose molecular structure is given in Fig. 2(aII). This intermediate state has an end-to-end extension from 3-6 nm as can be seen in Fig. 1 which agrees with the observation by Pappalardo *et al.* that in the region from 30 to 60 Å, HC continues to unfold and the two β-strands slide over each other.[34] At the same time, the native hydrogen bond
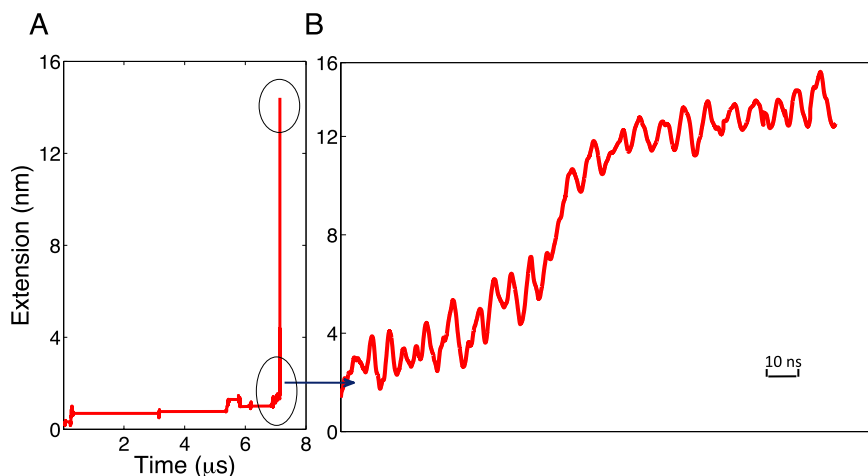

FIG. 1. (a) End-to-end extension as a function of time for 100 pN clamping forces of WT PrP as obtained using the SLME method. (b) Zoom in detailing the lifetime of the intermediate configurations; result represents an average over 15 simulations.
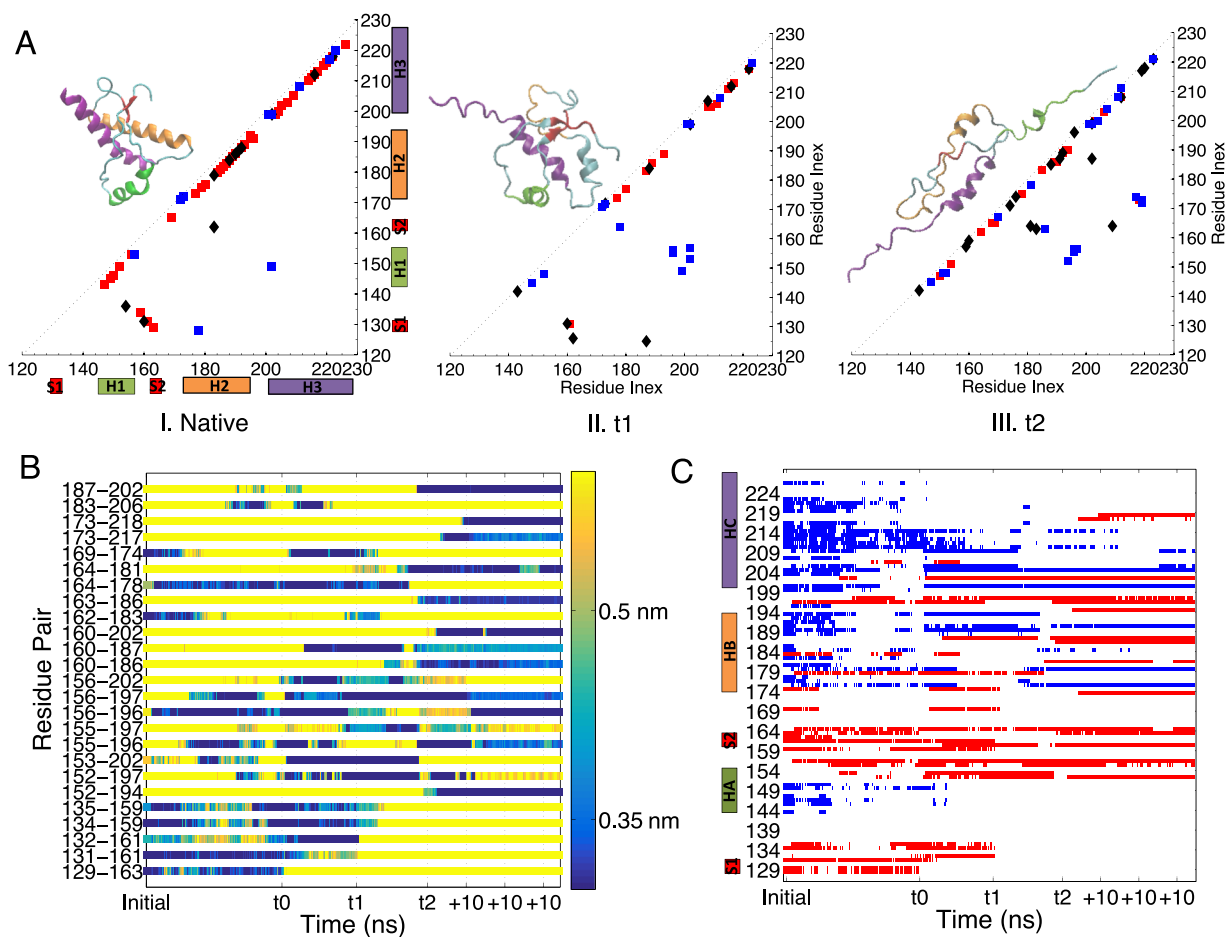
FIG. 2. Analysis of unfolding pathway involving three-stranded intermediate configuration for wild-type PrP at 100 pN clamping force. (aI) shows the contact map and molecular structure of native configuration which contains three α-helices: HA (residues 144-156), HB (residues 172-194), HC (residues 200-228), and a short β-sheet (S1 residues 129-132 and S2 residues 160-163), colored in green, orange, purple, and red, respectively. Each marker denotes a contact. Main chain-main chain contacts are represented with red squares, main chain-side chain contacts with black diamonds, and side chain-side chain contacts with blue squares. All the hydrogen bonds are viewed in VMD with a distance cutoff of 3 Å and an angle cutoff of 30°. (aII) shows the intermediate configuration that emerges during the breakage of the native β-sheet at an extension of about 3 nm, while (aIII) shows the three-stranded intermediate configuration forming at t_2 ($t_1 + 5$ ns) at an extension of about 13.5 nm. The native β-sheet unravels at around 6 μs (t_0) and the first intermediate configuration shown in (aII) breaks at t_1 which is 10 ns after t_0. (b) Inter-residue distances as a function of time between residues that are involved in the formation of the three-stranded intermediate configuration. (c) Secondary structure of each residue as a function of simulation time. Blue represents the α-helix structure, while red represents the β-sheet or β-sheet-like structure.

Y162-T183 breaks and subsequently, salt bridges R156-E196 and R164-D178 form, which stabilizes the interaction between the S2 region (residues 155-171) and HB (residues 172-194).

The second intermediate state at 13 nm extension, which emerges at t_2 that is 5 ns after the unfolding of the first intermediate configuration at t_1, is more interesting and represents a three-stranded structure containing residues 155-214 as can be seen in Fig. 2(aIII). The core of this conformation is a β-sheet-like structure including the S2 region and HB, which are linked by newly formed hydrogen bonds. Following the disruption of the extended β-sheet, HA which is part of the native 20-residue hydrophobic core composed of 13 residues from HB-HC and 4 residues from HA,[35] gradually rotates away from the HB-HC region. Subsequently, there is a progressive loss of helicity in HA and the N-terminus of HB as can be seen in Fig. 2(c). Simultaneously, a number of hydrogen bonds are formed between the S2 region and the unwound HB which results in a β-sheet-like structure. Together with the HB-HC core, which is linked by the disulfide bridge, the β-sheet-like structure comprises a three-stranded configuration.

Fig. 2(b) shows the inter-residue distances between the most populated residues involved in the intermediate configurations. The R156-E196 and R164-D178 salt bridges, which form in the very early stages of the unfolding process, link the S2 region to HB and play an essential role in the formation of the three-stranded intermediate states. These salt bridges were also observed in several independent MD studies[13,36] in which the pH was varied. The M129-Y163 and G131-V161 pairs existing in the native β-sheet break at t_0, which is around 6 μs. The newly formed hydrogen bonds S132-V161, M134-N159, and S135-N159, which extend the native β-sheet, break at t_1 which is 10 ns after t_0. At t_2, that is 5 ns after t_1, a number of new hydrogen bonds start to form between the S2 region and HB, which leads to the formation of the three-stranded intermediate state.

We note that we name the three stranded core as a β-sheet-like structure rather than a β-sheet since the hydrogen bonds are mostly formed between atoms on the side chains, rather than between backbone atoms as shown in Fig. 2(aIII). The number of residues involved in the β-sheet-like content

increases from 4 (3.8%, M129-Y163 and G131-V161) to 40 (38.1%, residues 155-195) while the α-helix content decreases to 20 residues (19%, partial of HB (residues 179-189) and HC (residues 205-214)) from 60 residues (57.1%), which is in line with the structural range of 17%-30% α-helix and 43%-54% β-sheet as observed in experimental studies of PrP^{Sc}.[3,4] Furthermore, the location of the three-stranded structure is in agreement with the suggestion that the H2-H3 domain may act as a conformational switch in the full protein.[37] In particular, Cobb *et al.* observed a tightly packed core located at residues $\approx$160-220 when using site-directed spin labeling and EPR spectroscopy to study a misfolded PrP amyloid.[33] Also, a single-molecule force spectroscopy study has reported the existence of a β-sheet core starting at residues $\approx$164-169 of PrP amyloid according to its force-extension curve, which is consistent with our results.[19]

We also discuss the seeming discrepancy between the large percentage of intermediate configurations observed in this work at 100 pN clamping force, which is in contrast to the nearly universal two state unfolding that was observed experimentally by Yu *et al.*[16] at 10 pN. As seen in Fig. 1(b), the survival time of the three-stranded intermediate state at 100 pN clamping force is up to hundreds of nanoseconds, which is much smaller than the experimental resolution of 50-100 μs.[17] The survival times were computed using Eq. (A2) in the Appendix, where the height of the energy barriers that are crossed can be computed directly from the SLME method and where the prefactor for the transition state expression in Eq. (A2) is obtained directly from recent experimental studies on single molecule unfolding of PrP.[16]

As mentioned above, the three-stranded intermediate configuration is stable and maintains its configuration after tens of nanoseconds under 100 pN clamping force. Its stability is governed by three factors. First, the direction of pulling results in a shear of the β-strands, which requires a much larger force to separate than does a peeling mode.[38] Second, we observe the formation of an average of 12 new hydrogen bonds in the three-stranded core as can be seen in Fig. 2(b). Most residues involved in the polar contacts of the intermediate configuration are charged residues such as R156, R164, E167, K194, E187, and D202. Also the hydrophobic effect in the HB-HC region stabilizes the intermediate configuration. Finally, a special constraint is imposed by the presence of the native disulfide bridge between C179 and C214, which requires a substantial amount of force, reported to be larger than 1000 pN,[39] to break.[40] Consequently, the force carried by HB and HC is significantly reduced due to the presence of the disulfide bridge. A similar effect of the disulfide bond was reported in the constant strain rate MD studies of PrP by Pappalardo *et al.*,[34] where the unfolding force reached 5000 pN for an extension of 10 nm, which also supports our conclusion regarding the stability of the three-stranded intermediate configuration under 100 pN clamping force.

B. Mutant PrP

Recently, it was reported that removing the disulfide bond will result in conformational changes similar to the effect of low pH denaturing condition and may lead to the misfolding

of PrP.[41] Also, the removal of the disulfide bridge by mutating C179 and C214 to Ala is known to promote aggregation and β-structure formation upon oligomerization.[42] To investigate how the unfolding pathway will change and whether the three-stranded intermediate state still forms without the existence of the disulfide bridge, we study the unfolding of a mutated huPrP, C179A/C214A. As shown in Fig. S4(b),[49] the unfolding times in the high force regime (i.e., $\geq$200 pN) for mutant huPrP obtained using the SLME method is in the same order as those obtained from the SMD simulations. The unfolding pathway reveals a two state unfolding (see Fig. S3 of the supplementary material)[49] with an end-end extension of 26.5 nm for the unfolded state.

Here, as in the case of WT PrP, we concentrate on the unfolding of mutant PrP under the clamping force of 100 pN. The first unfolding pathway, as shown in Fig. 3 for a 100 pN clamping force, starts with the breakage of the native β-sheet and the subsequent unfolding of HC. The polar contacts H155-D196 and R156-D196, which form in the early stage of the unfolding process, connect the S2 region to HB while the Y157-D202 hydrogen bond stabilizes the interaction between HC and the S2 region as shown in Fig. 4(b). After the breakage of native β-sheet happening at t_0' (around 8 ns), the S2 region gradually rotates to lie parallel to HB and HC. As a result, a number of hydrogen bonds form among residues 155-214 and a three-stranded intermediate configuration emerges as illustrated in Fig. 4(b). Different from the three-stranded structure described previously in Fig. 2(aIII) for WT PrP, HC is linked with HB by hydrogen bonds but not by the disulfide bridge, as illustrated in Fig. 4(aIII). The end-to-end extension of the intermediate state is around 15 nm which is slightly larger than that of the WT protein (13.5 nm) since HC loses most of its helical structure due to the removal of the disulfide bridge during the unfolding process of mutant PrP as described in Fig. 4(c). The three-stranded intermediate state follows an α-β-α motif where HC is unwound and the major part of HB maintains its helical configuration as illustrated in Fig. 4(aIII).

The unfolding along pathways 2(a) and 2(b) in Fig. 5 are very similar. They both begin with the unfolding of HC as illustrated in Fig. 5(b). Similar to what we observed in the WT PrP unfolding at 100 pN clamping force, newly formed hydrogen
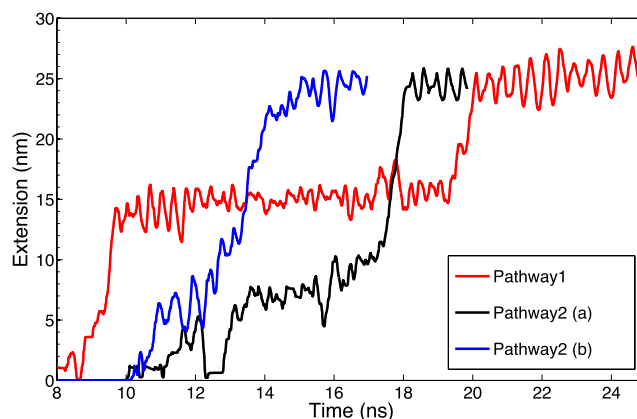

FIG. 3. End-to-end extension as a function of time at 100 pN clamping forces for two most common unfolding pathways of C179A/C214A mutant PrP obtained using the SLME method.
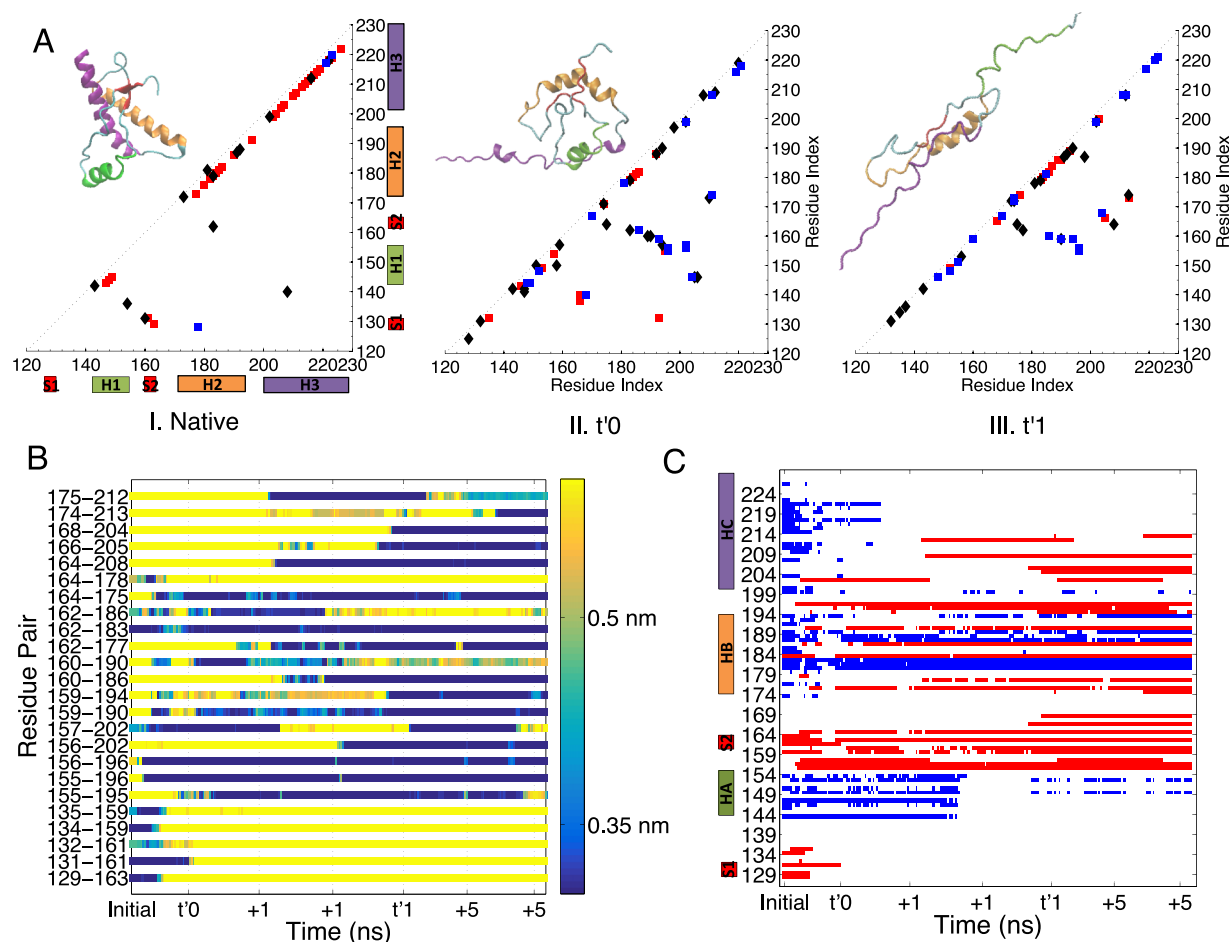
FIG. 4. Analysis of unfolding pathway 1 from Fig. 3 for C179A/C214A mutant PrP at 100 pN clamping force. (aI) shows the contact map and molecular structure of native configuration. (aII) shows the unfolding of HC and separation of native β-sheet at around 13 ns (t'_0) with intermediate configuration happening at t'_1 ($t'_0 + 3$ ns) shown in (aIII). (b) Inter-residue distances as a function of time between residues that are involved in the formation of the three-stranded intermediate configuration. (c) Secondary structure of each residue as a function of simulation time. Blue represents the α-helix structure, while red represents the β-sheet or β-sheet-like structure.

bonds L130-Y163, S132-V161, and M134-N159 extend the native β-sheet structure as can be seen in Fig. 5(b). However, the mechanism by which the native β-sheet breaks influences the time spent in the intermediate state with extension around 7.5 nm. Specifically, for pathway 2(b), the β-sheet unfolds in a peeling mode. In contrast, for pathway 2(a), the β-sheet unravels in a shear mode. The shear mode results in a longer time spent in the intermediate state at 7.5 nm extension, of about 4 ns as compared to 2 ns for pathway 2(a). Furthermore, in contrast to the WT unfolding, HC unfolds much earlier than the breakage of the β-sheet region as shown in Fig. 5(b). Thus, while the intermediate state for the WT PrP at 100 pN force shown in Fig. 1 is the same as that shown for both pathways 2(a) and 2(b) in Fig. 3, the extension in the mutant PrP case is longer (7.5 nm) as compared to the shorter (3 nm) extension for the WT PrP intermediate state.

Among the 60 SLME simulations with clamping force of 100 pN for mutant PrP, 38 cases follow the second pathway, among which 15 cases follows pathway 2(a). The other 23 cases following the second pathway show two-state unfolding as illustrated in pathway 2(b) in Fig. 3. All of the first pathway simulations pass through the three-stranded intermediate state. The observation of the three-stranded intermediate state in the mutant PrP unfolding suggests that it is possible for the

C179A/C214A mutant to convert into β-sheet-rich form under the function of applied clamping force.

The three-stranded intermediate states found in our simulations of both WT and mutant PrP match well with other reported studies. Recent experimental studies[16] have reported a transition state of PrP folding (probably without the disulfide bond) using an energy landscape analysis, retaining most of HB and HC, the adjacent loop, and β2, which matches the intermediate states observed in our simulations as can be seen in Figs. 2(aIII) and 4(aIII). By measuring folding trajectories of single WT PrP and C179A/C214A mutant molecules, Yu *et al.*[16] observed three misfolded configurations M1 (7.1 $\pm$ 0.4 nm from unfolded state), M2 (10.5 $\pm$ 0.5 nm from unfolded state), and M3 (4.9 $\pm$ 0.2 nm from unfolded state), among which M1 has the highest occupancy. The intermediate state observed in our SLME simulations under 100 pN of WT PrP is 6 $\pm$ 0.5 nm from the unfolded state as shown in Fig. 1, which agrees with M1 while the intermediate configuration for mutant PrP under 100 pN clamping force is 10.5 $\pm$ 0.5 nm from the unfolded state (i.e., the intermediate exists around 15 nm extension) as illustrated in Fig. 3, which agrees with M2.

Furthermore, the intermediate states observed in our simulation allow us to identify the folding motif for the PrP amyloid. The three-stranded intermediate configuration can form a

A

I. t″0   II. t″1

B

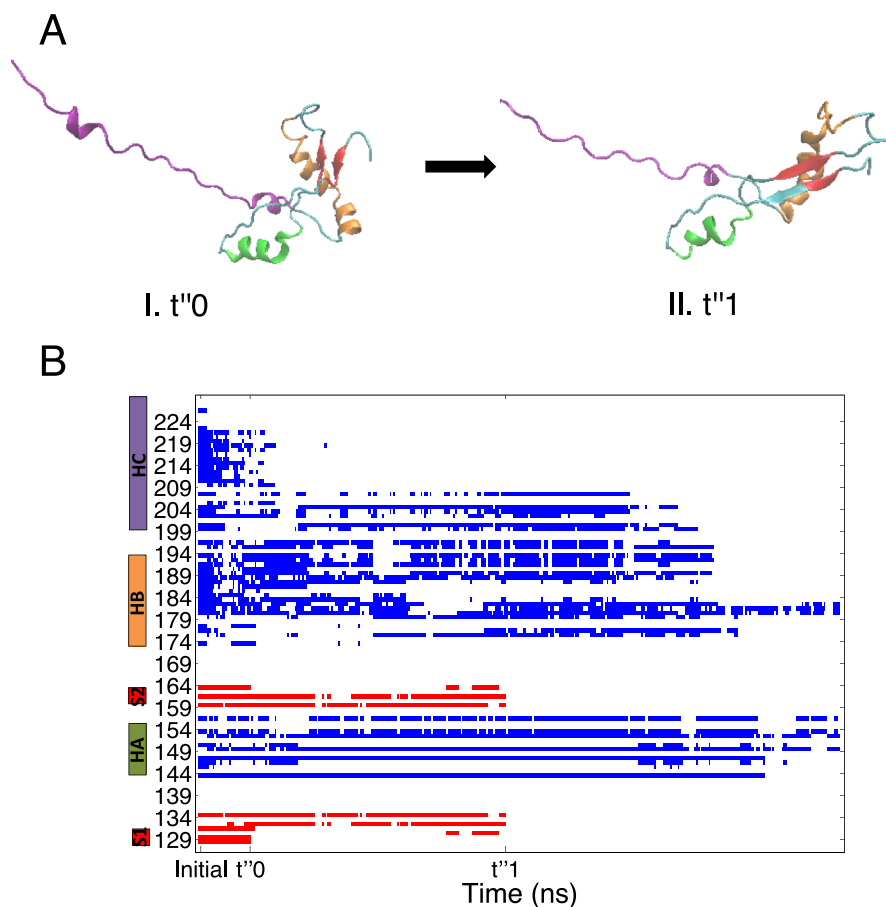Initial t″0   t″1

Time (ns)

FIG. 5. (a) Molecular structure representing the unfolding pathway 2(a) from Fig. 3 for C179A/C214A mutant PrP at 100 pN clamping force. (aI) shows the unfolding of HC and separation of native β-sheet happening at around 13 ns (t_0'') while the intermediate configuration unfolding at t_1'' ($t_0'' + 5$ ns) is shown in (aII). (b) Secondary structure of each residue as a function of simulation time. Blue represents the α-helix structure, while red represents the β-sheet or β-sheet-like structure.

β-helix model by connecting adjacent monomers to each other by head to head and tail to tail. Dong *et al.* have also proposed a β-helix model of NM fibrils when studying the unfolding of the amyloid fibrils.[43] Also, the stability of the three-stranded intermediate configuration under 100 pN clamping force can explain why the discontinuities in force-extension trace of NM fibrils exist only at unusually high pulling force (larger than 250 pN) reported by Dong *et al.*[43]

We can further compare our simulations with previous experiments, for example, those of Dong *et al.*[43] by comparing the barrier width along the energy pathway between the folded and unfolding configurations. We do this by utilizing the force-dependent unfolding times shown in Fig. S4[49] and using Bell's

equation, which is defined as $t(F) = t_0 \exp(-F\Delta x/K_B T)$, where t_0 is the intrinsic lifetime without clamping force and Δx denotes the barrier width. By fitting the force dependent unfolding time of WT PrP using Bell's formula, we obtain $\Delta x = 0.0911 \pm 0.013$ nm. This barrier width is comparable to the value obtained by Dong *et al.* as $\Delta x = 0.13 \pm 0.01$ nm[43] while the slight differences can be attributed to the fact that we performed unfolding simulations of a single prion protein, while the work by Dong *et al.* considered the unfolding of a prion fibril.

Finally, in Fig. 6, we show the potential of mean force (PMF) for the three-stranded intermediate configurations observed in both the wild-type PrP and mutant PrP simulation at
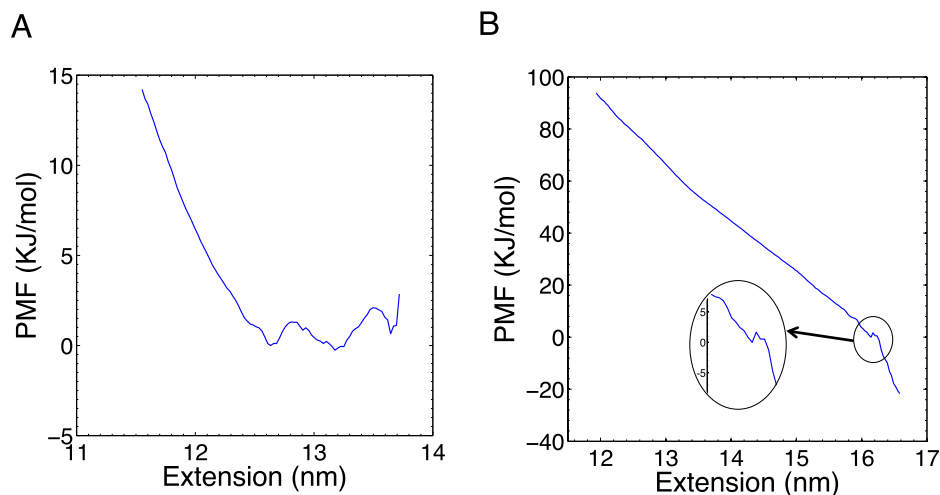
A

B

FIG. 6. PMF as a function of extension for 3-stranded core for both the (a) wild-type PrP and (b) mutant PrP at 100 pN clamping force.

100 pN calculated using umbrella sampling (see the Appendix for details). The free energy barrier for the three-stranded intermediate configuration of WT PrP (about 3 kJ/mol) shown in Fig. 6(a) is three times higher than that of the mutant PrP (about 1 kJ/mol) provided in Fig. 6(b). This is consistent with the lifetime of intermediate state discussed above. Due to having a higher energy barrier to overcome, the lifetime of the intermediate state of WT PrP is ten times longer than that of the mutant as seen in Figs. 1 and 3. Here, we note that the shape of the PMF for mutant PrP is independent of the unfolding pathways. It is also important to note that these free energy barriers are similar to the energy of thermal fluctuation, which implies that prion protein can undergo the transition to the β-sheet-like structure and back under equilibrium conditions. This has in fact been observed experimentally in the work of Yu *et al.*,[16] (see Figure 3 in that work, for example), where such transitions between the unfolded and intermediate configurations are shown to frequently occur.

III. CONCLUSION

In conclusion, we have utilized a recently developed atomistic method that couples potential energy surface exploration and applied mechanical force to study the unfolding of PrP. Our key finding is that we have directly observed the transition of the prion from its native, α-rich structure into a partially unfolded, β-rich form through the formation of a three-stranded β-sheet-like intermediate configuration. By directly observing this transition, we have found support to the structural theory that there is a core of amyloid fibrils of human PrP mapping to C-terminal residues from 160-220. This β-sheet-like structure was also observed when the disulfide bond is mutated, which suggests that residues 155-194 may play a key role in the formation of PrP^{Sc}. Moreover, the intermediate states we have found match those previously reported for PrP without the disulfide bond, which demonstrates the potential of using mechanical force to elucidate the unfolding and misfolding mechanisms in PrP. Our work sheds light on the important role of force on the formation of aggregation-prone intermediate conformation for prion proteins.

APPENDIX: SELF-LEARNING METABASIN ESCAPE ALGORITHM

It is well-known that SMD simulations for force clamping exhibit two major drawbacks as compared to the corresponding force clamp experiments. First, the SMD simulations are typically performed at constant applied forces (i.e., greater than 250 pN) that are much larger than those used experimentally (10-100 pN) for prion protein. Thus, the energy landscape explored during SMD simulations is likely to be significantly different than that in the experiments.[17] Second, steered MD simulations can only access time scales on the order of hundreds of nanoseconds, which is nearly 10 orders of magnitude smaller than the experimentally observed unfolding time of seconds.[17]

In order to study the unfolding of ubiquitin at experimentally relevant forces and time scales, we utilize the recently developed SLME method of Cao *et al.*[29,30] which couples potential energy surface (PES) exploration with mechanical deformation and which was recently used to give new insights into the unfolding pathways and intermediate configurations of ubiquitin.[31] In this approach, quartic penalty functions ϕ_p are utilized to push the system out of potential energy wells in which it can become stuck due to the relatively low force (100 pN) that is constantly applied. The modified potential energy can be written as

$$\Psi(\mathbf{r}) = E(\mathbf{r}) + \sum_{i=1}^{p} \phi_P(\mathbf{r}), \qquad (A1)$$

where $\Psi(\mathbf{r})$ is the augmented potential energy due to the addition of the penalty functions ϕ_p, $E(\mathbf{r})$ is the original potential energy function, i.e., the bLJ potential in the present case, and p is the total number of penalty functions. The force on each atom can then be obtained as is done in molecular simulations by taking the gradient of the augmented potential energy Ψ in Eq. (A1).

Upon application of a sufficient number of penalty functions, the system escapes over the lowest energy barrier to a neighboring potential energy well, where penalty functions are again applied if the applied force is not sufficient to lower the energy barrier to enable the system to escape. Thus, the penalty functions can be physically interpreted as thermal activation that assists the mechanical force in enabling the system to escape from a local energy minimum. This procedure is repeated until PrP is completely unfolded for the wide type resulting in an end-end distance around 19 nm and for mutant PrP resulting in an end-to-end extension around 26.5 nm. In going through this procedure, the system is able to find and pass through all relevant intermediate configurations, which are described in the main manuscript.

We employed the AMBER99sb potential field[44] which utilizes an implicit solvent model for water in conjunction with the Protein Data Bank (PDB) ID 1HJM for the native configuration of PrP^C. The native prion protein structure was equilibrated at 300 K, and then energy minimization was performed to generate the corresponding local energy minimum. At both the N and C-termini, we applied a constant pulling force ranging from 100 to 600 pN using the SLME method. Clamping forces greater than 200 pN were also simulated using SMD to compare with the result of SLME at high force range. All simulations, i.e., both SMD and SLME, were performed using the open source GROMACS simulation package.[45]

Based on the transition state theory,[46,47] we calculate the unfolding time (τ) of the SLME method via

$$\tau = \left(\nu \exp^{-Q/k_B T}\right)^{-1}, \qquad (A2)$$

where Q is the activation energy barrier separating two adjacent energy minima, ν is a frequency prefactor, and T is the

temperature. To use the transition state theory, the energy barriers Q can be obtained directly from the SLME simulations, but the issue remains how to find the prefactor ν. In this work, we use the experimentally obtained values by Yu *et al.*[16] There, they obtained, for temperature T = 300 K, an unfolding force of F = 9.1 ± 0.1 pN, and δx = 10.4 ± 0.6 nm, for which the unfolding time $\tau = 3 \times 10^2 \pm 0.4$ μs. Solving for ν with those experimental values gives a value of $\nu = 4 \times 10^{12}$ s^{-1}. While the values of the frequency prefactor are likely to be different for WT and mutant PrP, we have used the same value of $\nu = 4 \times 10^{12}$ s^{-1} in the present work due to the lack of experimental results distinguishing ν for WT and mutant PrP.

For obtaining the PMF, we did umbrella sampling with 100 pN clamping force. The umbrella sampling was done every 0.05 nm at a force constant of 800 kJ mol^{-1} nm^{-2} for WT PrP and 100 kJ mol^{-1} nm^{-2} for mutant PrP. We obtained overlapped histograms between adjacent windows, and the PMF was extracted by the Weighted Histogram Analysis Method (WHAM).[48]

[1] S. B. Prusiner, "Prions," Proc. Natl. Acad. Sci. U. S. A. **95**, 13363–13383 (1998).

[2] C. M. Dobson, "The structural basis of protein folding and its links with human disease," Philos. Trans. R. Soc. London, Ser. B **356**, 133–145 (2001).

[3] B. W. Caughey, A. Dong, K. S. Bhat, D. Ernst, S. F. Hayes, and W. S. Caughey, "Secondary structure analysis of the scrapie-associated protein PrP 27-30 in water by infrared spectroscopy," Biochemistry **30**, 7672–7680 (1991).

[4] K.-M. Pan, M. Baldwin, J. Nguyen, M. Gasset, A. Serban, D. Groth, I. Mehlhorn, Z. Huang, R. J. Fletterick, and F. E. Cohen, "Conversion of alpha-helices into beta-sheets features in the formation of the scrapie prion proteins," Proc. Natl. Acad. Sci. U. S. A. **90**, 10962–10966 (1993).

[5] R. Riek, S. Hornemann, G. Wider, M. Billeter, R. Glockshuber, and K. Wüthrich, "NMR structure of the mouse prion protein domain PrP (121-231)," Nature **382**, 180–182 (1996).

[6] R. Zahn, A. Liu, T. Lührs, R. Riek, C. von Schroetter, F. L. García, M. Billeter, L. Calzolai, G. Wider, and K. Wüthrich, "NMR solution structure of the human prion protein," Proc. Natl. Acad. Sci. U. S. A. **97**, 145–150 (2000).

[7] L. Calzolai and R. Zahn, "Influence of pH on NMR structure and stability of the human prion protein globular domain," J. Biol. Chem. **278**, 35592–35596 (2003).

[8] B. Caughey, G. S. Baron, B. Chesebro, and M. Jeffrey, "Getting a grip on prions: Oligomers, amyloids, and pathological membrane interactions," Annu. Rev. Biochem. **78**, 177–204 (2009).

[9] N. J. Cobb and W. K. Surewicz, "Prion diseases and their biochemical mechanisms," Biochemistry **48**, 2574–2585 (2009).

[10] R. Diaz-Espinoza and C. Soto, "High-resolution structure of infectious prion protein: The final frontier," Nat. Struct. Mol. Biol. **19**, 370–377 (2012).

[11] S. R. R. Campos, M. Machuqueiro, and A. M. Baptista, "Constant-pH molecular dynamics simulations reveal a β-rich form of the human prion protein," J. Phys. Chem. B **114**, 12692–12700 (2010).

[12] P. Baillod, J. Garrec, M.-C. Colombo, I. Tavernelli, and U. Rothlisberger, "Enhanced sampling molecular dynamics identifies PrP^{sc} structures harboring a c-terminal β-core," Biochemistry **51**, 9891–9899 (2012).

[13] M. L. DeMarco and V. Daggett, "Molecular mechanism for low pH triggered misfolding of the human prion protein," Biochemistry **46**, 3045–3054 (2007).

[14] M. W. van der Kamp and V. Daggett, "Influence of pH on the human prion protein: Insights into the early steps of misfolding," Biophys. J. **99**, 2289–2298 (2010).

[15] M. L. DeMarco and V. Daggett, "From conversion to aggregation: Protofibril formation of the prion protein," Proc. Natl. Acad. Sci. U. S. A. **101**, 2293–2298 (2004).

[16] H. Yu, A. N. Gupta, X. Liu, K. Neupane, A. M. Brigley, I. Sosova, and M. T. Woodside, "Energy landscape analysis of native folding of the prion protein yields the diffusion constant, transition path time, and rates," Proc. Natl. Acad. Sci. U. S. A. **109**, 14452–14457 (2012).

[17] H. Yu, D. R. Dee, and M. T. Woodside, "Single-molecule approaches to prion protein misfolding," Prion **7**, 140–146 (2013).

[18] H. Yu, X. Liu, K. Neupane, A. N. Gupta, A. M. Brigley, A. Solanki, I. Sosova, and M. T. Woodside, "Direct observation of multiple misfolding pathways in a single prion protein molecule," Proc. Natl. Acad. Sci. U. S. A. **109**, 5283–5288 (2012).

[19] D. N. Ganchev, N. J. Cobb, K. Surewicz, and W. K. Surewicz, "Nanomechanical properties of human prion protein amyloid as probed by force spectroscopy," Biophys. J. **95**, 2909–2915 (2008).

[20] K. C. Neuman and A. Nagy, "Single-molecule force spectroscopy: Optical tweezers, magnetic tweezers and atomic force microscopy," Nat. Methods **5**, 491 (2008).

[21] C. Bustamante, Y. R. Chemla, N. R. Forde, and D. Izhaky, "Mechanical processes in biochemistry," Annu. Rev. Biochem. **73**, 705–748 (2004).

[22] E. Paci and M. Karplus, "Unfolding proteins by external forces and temperature: The importance of topology and energetics," Proc. Natl. Acad. Sci. U. S. A. **97**, 6521–6526 (2000).

[23] J. Ma, R. Wollmann, and S. Lindquist, "Neurotoxicity and neurodegeneration when PrP accumulates in the cytosol," Science **298**, 1781–1785 (2002).

[24] R. I. Dima and D. Thirumalai, "Probing the instabilities in the dynamics of helical fragments from mouse PrP^c," Proc. Natl. Acad. Sci. U. S. A. **101**, 15335–15340 (2004).

[25] A. O. Samson and M. Levitt, "Normal modes of prion proteins: From native to infectious particle," Biochemistry **50**, 2243–2248 (2011).

[26] A. Barducci, R. Chelli, P. Procacci, V. Schettino, F. L. Gervasio, and M. Parrinello, "Metadynamics simulation of prion protein: β-structure stability and the early stages of misfolding," J. Am. Chem. Soc. **126**, 2705–2710 (2006).

[27] M. Sotomayor and K. Schulten, "Single-molecule experiments in vitro and in silico," Science **316**, 1144–1148 (2007).

[28] A. Zhmurov, O. Kononova, R. I. Litvinov, R. I. Dima, V. Barsegov, and J. W. Weisel, "Mechanical transition from α-helical coiled coils to β-sheets in fibrin(ogen)," J. Am. Chem. Soc. **134**, 20396–20402 (2012).

[29] P. Cao, M. Li, R. J. Heugle, H. S. Park, and X. Lin, "Self-learning metabasin escape algorithm for supercooled liquids," Phys. Rev. E **86**, 016710 (2012).

[30] P. Cao, H. S. Park, and X. Lin, "Strain-rate and temperature-driven transition in the shear transformation zone for two-dimensional amorphous solids," Phys. Rev. E **88**, 042404 (2013).

[31] P. Cao, G. Yoon, W. Tao, K. Eom, and H. S. Park, "The role of binding site on the mechanical unfolding mechanism of ubiquitin," Sci. Rep. **5**, 8757 (2015).

[32] A. Kushima, X. Lin, J. Li, J. Eapen, J. C. Mauro, X. Qian, P. Diep, and S. Yip, "Computing the viscosity of supercooled liquids," J. Chem. Phys. **130**, 224504 (2009).

[33] N. J. Cobb, F. D. Sönnichsen, H. Mchaourab, and W. K. Surewicz, "Molecular architecture of human prion protein amyloid: A parallel, in-register β-structure," Proc. Natl. Acad. Sci. U. S. A. **104**, 18946–18951 (2007).

[34] M. Pappalardo, D. Milardi, D. Grasso, and C. La Rosa, "Steered molecular dynamics studies reveal different unfolding pathways of prions from mammalian and non-mammalian species," New J. Chem. **31**, 901–905 (2007).

[35] R. Riek, G. Wider, M. Billeter, S. Hornemann, R. Glockshuber, and K. Wüthrich, "Prion protein NMR structure and familial human spongiform encephalopathies," Proc. Natl. Acad. Sci. U. S. A. **95**, 11667–11672 (1998).

[36] J. Zuegg and J. Gready, "Molecular dynamics simulations of human prion protein: Importance of correct treatment of electrostatic interactions," Biochemistry **38**, 13862–13876 (1999).

[37] Z. Xu, S. Prigent, J.-P. Deslys, and H. Rezaei, "Dual conformation of H2H3 domain of prion protein in mammalian cells," J. Biol. Chem. **286**, 40060–40068 (2011).

[38] D. J. Brockwell, E. Paci, R. C. Zinober, G. S. Beddard, P. D. Olmsted, D. A. Smith, R. N. Perham, and S. E. Radford, "Pulling geometry defines the mechanical resistance of a β-sheet protein," Nat. Struct. Mol. Biol. **10**, 731–737 (2003).

[39] S. Keten, C.-C. Chou, A. C. T. van Duin, and M. J. Buehler, "Tunable nanomechanics of protein disulfide bonds in redox microenvironments," J. Mech. Behav. Biomed. Mater. **5**, 32–40 (2012).

[40] P. Carl, C. H. Kwok, G. Manderson, D. W. Speicher, and D. E. Discher, "Forced unfolding modulated by disulfide bonds in the Ig domains of a cell adhesion molecule," Proc. Natl. Acad. Sci. U. S. A. **98**, 1565–1570 (2001).

[41] L. Ning, J. Guo, N. Jin, H. Liu, and X. Yao, "The role of Cys179–Cys214 disulfide bond in the stability and folding of prion protein: Insights from molecular dynamics simulations," J. Mol. Model. **20**, 1–8 (2014).

[42] N. R. Maiti and W. K. Surewicz, "The role of disulfide bridge in the folding and stability of the recombinant human prion protein," J. Biol. Chem. **276**, 2427–2431 (2001).

[43]J. Dong, C. E. Castro, M. C. Boyce, M. J. Lang, and S. Lindquist, "Optical trapping with high forces reveals unexpected behaviors of prion fibrils," Nat. Struct. Mol. Biol. **17**, 1422–1430 (2010).

[44]V. Hornak, R. Abel, A. Okur, B. Strockbine, A. Roitberg, and C. Simmerling, "Comparison of multiple Amber force fields and development of improved protein backbone parameters," Proteins: Struct., Funct., Bioinf. **65**, 712–725 (2006).

[45]B. Hess, C. Kutzner, D. Van Der Spoel, and E. Lindahl, "GROMACS 4: Algorithms for highly efficient, load-balanced, and scalable molecular simulation," J. Chem. Theory Comput. **4**, 435–447 (2008).

[46]P. Hänggi, P. Talkner, and M. Borkovec, "Reaction-rate theory: Fifty years after Kramers," Rev. Mod. Phys. **62**, 251 (1990).

[47]I. Popa, J. M. Fernández, and S. Garcia-Manyes, "Direct quantification of the attempt frequency determining the mechanical unfolding of ubiquitin protein," J. Biol. Chem. **286**, 31072–31079 (2011).

[48]J. S. Hub, B. L. De Groot, and D. Van Der Spoel, "g_wham? A free weighted histogram analysis implementation including robust error and autocorrelation estimates," J. Chem. Theory Comput. **6**, 3713–3720 (2010).

[49]See supplementary material at http://dx.doi.org/10.1063/1.4931819 for the validation of SLME algorithm via comparison to SMD.